Augmentation of thermal performance of air cooler having semi-circular tubes of an inline arrangement

T.M. Almulla, M.W. Shawki, M.F. Abd Rabbo, Y.A. Al-Mashad, M.R. Salem

Mechanical Engineering Department, Faculty of Engineering at Shoubra, Benha University, Shoubra ,Cairo, Egypt

Abstract : This work is a phase in augmenting the cooling load of an air cooler, which is considered as a cross flow heat exchanger. Here, an air cooler of in-line semicircular tubes (SCTs) is proposed and tested at a wide range of the airflow and attack angles of their bases ($0° \leq \alpha \leq 90°$). Their performance is practically compared with that of complete circular tubes (CCTs). In the experiments, cold water is passed through the tubes while hot air is passed across the bundle. The yields state that converting the tubes to pair of SCT augments the cooling rate besides increasing the air pressure decay. In the ranges, $0° \leq \alpha \leq 60°$ and $60° \leq \alpha \leq 90°$, the heat load and flow pressure loss are increased and decreased with rising the base angle, respectively. Besides, the thermal performance indicator (TPI) is increased by growing the SCT angle in the domain $0° \leq \alpha \leq 60°$, while it is damped with widening the angle in the extent $60° \leq \alpha \leq 90°$. Furthermore, the results document that the maximum value of TPI is 1.93.

Keywords: Inline tubes; Semi-circular; Attack angle; Performance indicator.

1. Introduction

The progress of countries typically requires many manufactures, in which heat is exchanged via heat exchangers. Thus, growing their load rate will reduce the capital and operating costs in such applications [1, 2]. Air cooler is the most application of tube bundles in crossflow. Its hydrothermal characteristics is very important to be examined [2, 3]. In the history, hundreds of researchers considered the performance behaviour of tube banks. Using the relevant data presented up to 1933, Colburn [4] anticipated a simple correlation for the heat exchange load from staggered CCTs. This is followed by numerous works which presented earlier analyses on the flow and heat exchange behaviour through isothermal and isofluxed CCTs at different rows/pitch ratios [5-13]. Moawed [14] experimentally and numerically investigated the heat load of an airflow across an in-line single SCTs. The study covered several attack angles and transversal spaces of the tubes with constant heat flux conditions. Ibrahiem and Elsayed [15] experimentally extended this work for staggered configuration. Liu et al. [16] practically considered the effect of the transverse pitch of a flattened tube bundle equipped with vortex generators on the performance attributes. The runs reported that increasing the transversal pitch reduced the interactions of vortices generated by vortex generators, which augmented the heat exchange.Odabaee and Hooman [17] simulated the heat exchange from a metal foam enveloped CCT bank. This design supplied higher performance than the conventional finned-CCT bundle. Lavasani et al. [18] practically considered the thermal response from a cam shaped inline CCTs. The authors recorded an enhancement of 7-14% by increasing the longitudinal pitch ratio from 1.5 to 2. Lin et al. [19] accomplished simulations of the heat loading rate and flow outlines for a flow crossing finned CCTs with vortex generators. The planned method decreased the wake section in arrears the tubes, which increased the thermal performance. Lavasani et al. [20] studied the flow/thermal characteristics of a nanofluid across CCT and cam-shaped tube banks. The author recorded a decrease in the friction by >70% by using the cam-shaped tube bank. Wang et al. [21] prepared an experimental setup to evaluate the thermal action of CCTs combined with three different geometries as vortex

generation tools. Tian et al. [22] performed another simulation study for airflow across finned isothermal CCT bank; circular pin-fins were considered in that work. Song et al. [23] practically examined the heating rate of finned CCTs with vortices generators. It was reported an enhancement with accompanying smaller generators at lower Reynolds numbers.

Ahmed et al. [24] simulated the water-based nanofluid flow crossing isothermal staggered CCTs. The authors studied the impact of the spacing between the tubes beside the effect of nanoparticles' concentration. Xu et al. [25] visualized numerically the flow/heating behaviour of air flowing across an aligned tube bank of six rows of tubes, which were equipped with rectangular discrete fins on their surfaces. Dang et al. [26] practically tested the heating rate attributes of a flow crossing CCTs with/without fins combined with vortex generators/distributes. Lotfi and Sundén [27] introduced other simulations for the flow streamlines around finned staggered slotted elliptic tube banks. It was documented that this approach improved the heat exchange rate by 15%. Lindqvist and Naess [28] numerically considered the flow behaviour across a finned bundle of staggered CCTs. From the presented survey in the previous section, it is obvious that a series of studies were practically/ numerically completed to enhance the exchange load through tube banks. Numerous techniques were proposed by the researchers to achieve that. It is evident that there is no work tested the incorporation of pair of SCTs as a passive tool, which does not necessitate any direct contribution of external energy to achieve the required heat load [29-34]. The existing study experimentally investigates the hydrothermal performance of in-line pairs of CCT or SCT bank at different airflow rates across the tubes. The tests cover numerous attack angles of the SCTs' bases. A representation of the cross section of a pair of SCTs is revealed in Fig. 1.
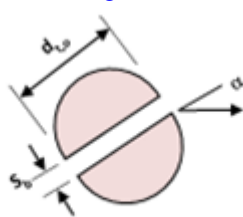

Fig. 1: A cross section of a pair of SCTs.

2. Experimental Apparatus

The apparatus used in the present investigation comprises two circuits; cooling water and heating air loops. The airflow stream considers an open-loop, which contains a suction-type air blower (5 hp), air obstruction,

orifice meter, transition duct, pressure sensors, test section with different configurations of the tubes, entrance tunnel, straightener, and air electric heater. The cooling water considers a closed cycle, which consists of a refrigeration circuit, valves, flow meter, pump, two collecting headers, the tested tube bank, and the pipes. Figs. 2 and 3 represent schematic diagrams of the experimental apparatus. The path of the airflow starts from the ingoing section. It comprises an air electric heater (6 kW) and a straightener. The action of the heater is controlled using a pre-adjusted thermostat to achieve a constant temperature of the air entering the tube bank. The galvanized steel tunnel (950 mm x 250 mm x 3500 mm); the outer surface is thermally isolated. After the entering segment, the air then passes over the test rig, at a distance of 2 m. Two headers are hinged in the vertical portion of the tunnel (250 mm x 300 mm). After leaving the main duct, the air enters the metering duct via a converging section. The metering part comprises an upstream PVC pipe, orifice plate, and downstream PVC pipe. The orifice plate is designed according to Miller [35]. A 5 hp centrifugal-type air suction blower is utilized to supply the system with air. The airflow rate is controlled via an airflow damper.

The cooling unit comprises100 litres insulated cabinet. The water is cooled in the cabinet by two coolers of ≈20 kW capacity. The running of the cooling unit is counted on a pre-set digital temperature regulator, which is utilized to possess a constant temperature of the water directed to the tubes. Besides, 3 hp pump is employed to circulate the water. The tested inline tube banks comprise 20 circular tubes or 40 semi-circular tubes; 5 rows and 4 columns. The dimensions of the examined arrangements are exposed in Fig. 4 and Table 1. The tubes are of copper of 15.88 mm and 1000 mm outside diameter and total length, respectively. To form SCTs, the CCT is cut longitudinally via a plasma cutting tool. Next, a cooper sheet is welded longitudinally to be its base. Fig. 5 presents a photo of a sample of the SCTs. Two cabinets are combined to accumulate the incoming water to/from the tubes. Totally, 16 wooden sheets of 4 mm wall thickness are employed as housing dies, placed between the header and duct nipples. These dies are drilled to provide holes for the tubes. Rubber gaskets are incorporated in each header to prevent any leakage. The CCTs/SCTs are connected to the two headers through the dies. Care is considered to seal off the gap that may be around the tubes in the die.
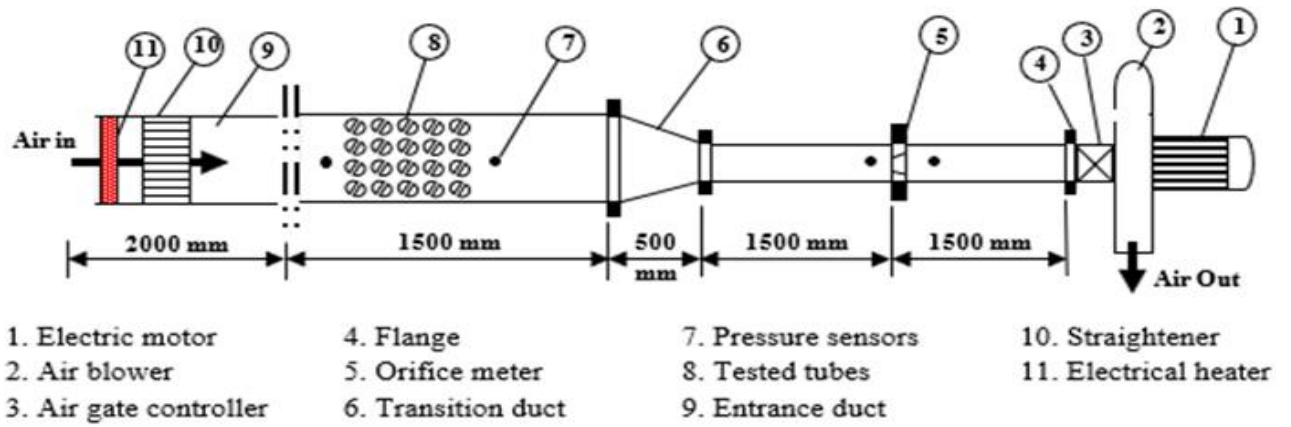
Air in

2000 mm   1500 mm   500 mm   1500 mm   1500 mm   Air Out

1. Electric motor   4. Flange   7. Pressure sensors   10. Straightener
2. Air blower   5. Orifice meter   8. Tested tubes   11. Electrical heater
3. Air gate controller   6. Transition duct   9. Entrance duct

Fig. 2: A schematic drawing of the heating air circuit.

Thermocouple

Water Flow Meter

Ball Valve

By-Pass Line

Ball Valve

Pump

Ball Valve

Cooling Unit

Drain
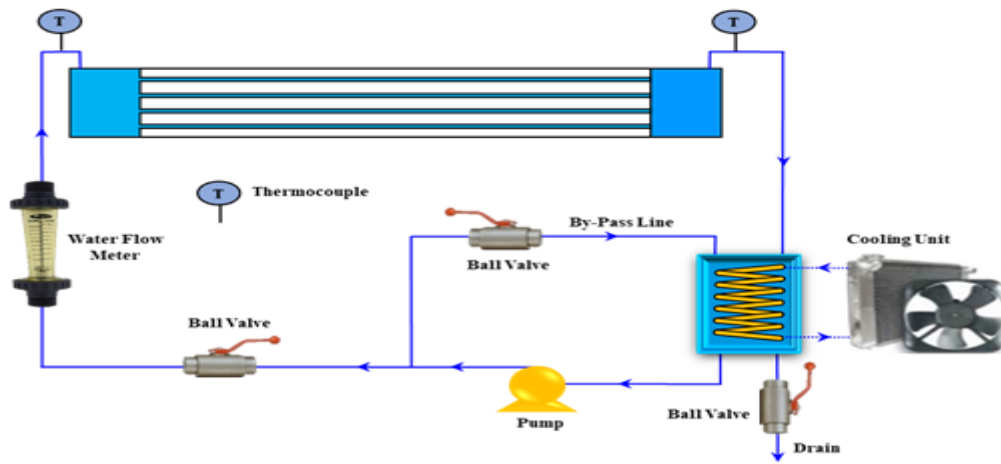
Fig. 3: A schematic drawing of the cooling water circuit.

Flow direction

S_b
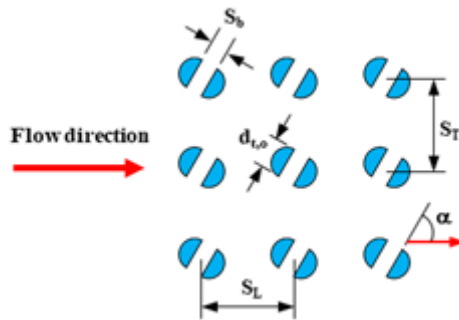
$d_{t,o}$

S_T

S_L

α

Fig. 4: Key dimensions of tested tube banks.
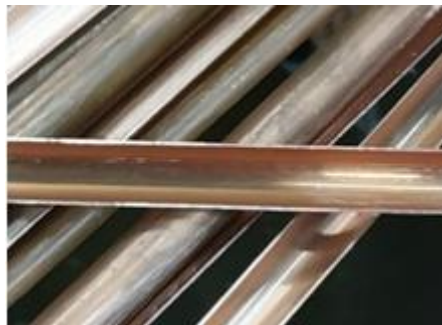
Fig. 5: Sample of incorporated SCTs

Table 1: Characteristic of the tested banks

No.	α (°)	S_b (mm)	δ	S_T (mm)	$S_T/d_{t,o}$	S_L (mm)	$S_L/d_{t,o}$
			Tube bank of CCTs				
1		———		31.75	2.0	31.75	2.0
			Tube banks of SCTs				
2 to 8	0, 15, 30, 45, 60, 75, 90	4	0.252	31.75	2.0	31.75	2.0

A variable area flowmeter, 10–100 l/min range and ±5% accuracy, is conducted to judge the flowing rate of the water. The air motion rate is estimated by measuring the floe resistance across the orifice plate by a digital manometer; ΔP ≤ 69 kPa, and accuracy of ±1 Pa. The same device estimates the pressure drop across the tested bundle. Eight K-type are utilized for assessing the inlet and outlet temperatures of both working fluids. Two of them are for the water, and the others for the air temperatures. All measuring devices are calibrated in the laboratory.

3. Test Procedures

To initiate the experiments, the blower, gate controller, orifice plate, convergent channel, testing section, main entering duct, straightener, heater, headers, examined bank, cooler, pump, pipes, flow meter, thermocouples, and the pressure transducer are coupled. Furthermore, the tubes are loaded and arranged in the duct according to the illustrated characteristics in Table 2. The first phase to collect the outputs from the system is to fill the cooling chamber with water. Then, the blower, heater, chiller, and pump are turned on. The temperatures of the fluids at entering are adjusted by regulating the heater/chiller thermostats. The water flowing rate is adjusted through the meter and the installed valves. While the airflow rate is controlled via the airflow damper. During the experiment running, the steady condition is presumed when a maximum alteration of 0.5°C within 25 minutes is recorded for each thermocouple.

Table 2: Range of fluids operational conditions

Parameters/operating conditions	Range or Value
Air-side	
Airflow rate, m³/s	0.285–1.677 (2170 ≤ $Re_{o,max}$ ≤ 12845)
Inlet temperature, °C	50±1 (Pr_o = 0.71)
Water-side	
Total water flow rate, l/min	61.2 (Re_i ≈ 3320)
Inlet temperature, °C	15 (Pr_i ≈ 7.94)

4. Thermal Performance Determination

In the heat exchange calculations, the primary measurements comprise six variables, namely the flow rates and inlet/outlet temperatures of both fluids. The heat exchange rates on the air and water sides (Q_o and Q_i) are calculated by;

$$Q_o = \dot{m}_o Cp_o (T_{a,ave,i} - T_{a,ave,o}) \tag{1}$$

$$Q_i = \dot{m}_i Cp_i (T_{w,o} - T_{w,i}) \tag{2}$$

For all tests, both loads calculated from the air and water sides do not differ by more than ±4% when compared with the average heat load (Q_{ave}). The overall thermal conductance is determined using Eq. (6). It should be noted that $\Delta T_{L.M}$ is calculated for counter flow configuration, while the correction factor F is assessed according to Shah and Sekulić [36]. For the tube walls, the conduction/fouling thermal resistances are disregarded. Therefore, the convection thermal resistances are employed to assess the overall transfer coefficient as follows;

$$U_o A_{t,o} = \frac{Q_{ave}}{F \, \Delta T_{L.M}} \tag{3}$$

$$\Delta T_{L.M} = \frac{(\Delta T_i - \Delta T_o)}{\ln \left[\frac{\Delta T_i}{\Delta T_o}\right]} \tag{4}$$

$$\frac{1}{U_i A_{t,o}} = \frac{1}{\overline{h}_o A_{t,o}} + \frac{1}{\overline{h}_i A_{t,i}} \tag{5}$$

Where $A_{t,o}$ is the tubes outer surface area, estimated as; ($A_{t,o} = 20\pi d_{t,o} L_t$) in the case of CCTs, and ($A_{t,o} = 40 d_{t,o} L_t (0.5\pi + 1)$) in the case of SCTs. For the inner surface, $A_{t,i}$ is evaluated based on $d_{t,i}$. The water flow through the tubes is turbulent fully developed. Consequently, the $\overline{Nu}_i$ is evaluated utilizing Gnielinski [37], Eq. (6), in which the Fanning friction factor is evaluated via Filonenko [38], Eq. (7). Then the average coefficient of heat transfer in the waterside is obtained.

$$\overline{Nu}_i = \frac{\frac{f_i}{2}(Re_i - 1000)Pr_i}{1 + 12.7\sqrt{\frac{f_i}{2}}\left(Pr_i^{2/3} - 1\right)}\left[1 + \left(\frac{d_{t,h}}{L_t}\right)^{2/3}\right] \tag{6}$$

$$f_i = 0.25(1.82 \log Re_i - 1.64)^{-2} \tag{7}$$

$$\overline{h}_i = \frac{\overline{Nu}_i . k_i}{d_{t,h}} \tag{8}$$

Where $d_{t,h}$ is the tube side hydraulic diameter, estimated as; ($d_{t,h} = d_{t,i}$) in the case of CCTs, and ($d_{t,h} = \pi d_{t,i}/(\pi + 2)$)in the case of SCTs. Now, the $\overline{Nu}_o$ for the air-side, can be obtained.

$$\overline{Nu}_o = \frac{\overline{h}_o d_{t,o}}{k_o} \tag{9}$$

The air velocity at the free space between the tubes ($u_{o,max}$) is obtained using its velocity in the free duct (u_o). then $Re_{o,max}$, St_o and f_o are

calculated. It should be noted that for all experimental runs, the average uncertainties in main parameters do not exceed 5.5%; as determined in Appendix A.

$$u_{o,max} = \frac{u_o \, S_T}{S_T - d_{t,o}} \qquad (10)$$

$$Re_{o,max} = \frac{u_{o,max} \, d_{t,o}}{\nu_o} \qquad (11)$$

$$St_o = \frac{\overline{Nu_o}}{Re_{o,max}.Pr_o} \qquad (12)$$

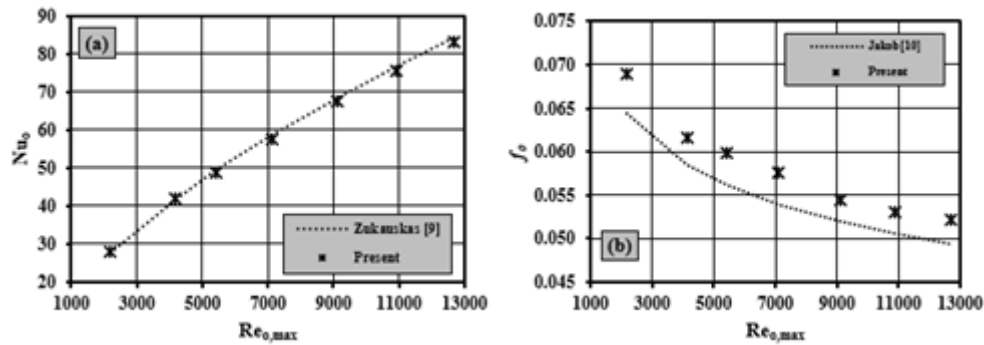$$f_o = \frac{\Delta P_o}{2 \, N_L \, \rho_o u_{o,max}^2} \qquad (13)$$

5. Apparatus validation and data verification

In the present study, Zukauskas [9], Eq. (14) and Jakob [10], Eq. (13) are conducted to verify the output data. The comparisons are done at the same working settings for inline circular tube case. The documented data for the $\overline{Nu_o}$ and f_o estimations are in good compatibility with established correlations by other authors with maximum differences of ±3.2% and ±6.9%, respectively.

$$\overline{Nu_o} = 0.2484 \, Re_{o,max}^{0.63} \, Pr_o^{0.36} \qquad (14)$$

$$f_o = \left[0.044 + \frac{0.08 * \frac{S_L}{d_{t,o}}}{\left(\frac{S_T}{d_{t,o}} - 1 \right)^{\left(0.43 + \frac{1.13 \, d_{t,o}}{S_L}\right)}} \right] Re_{o,max}^{-0.15} \qquad (13)$$

Fig. 6: Results of the apparatus validation; (a) $\overline{Nu_o}$, (b) f_o.

6. Results and discussions

6.1 Effect of SCT angle

Here, the purpose of this paper is achieved by documenting the hydrothermal performance of in-line SCT bank at different airflow rates (2170 ≤ R$_{eo,max}$ ≤ 12845) across the tubes with a constant temperature of 50°C (Pr$_o$ = 0.71). During the tests, several angles of the SCTs (0° ≤ α ≤ 90°) are considered. Furthermore, cooling water through the tubes is of constant temperature and total flow rate of 15°C (Pr$_i$ ≈ 7.94) and 61.2 l/min (Re$_i$ ≈ 3320), respectively. The tubes are arranged with constant S$_T$/d$_{t,o}$ = S$_L$/d$_{t,o}$ = 2.0 and δ = 0.252.

The results display that the hydrothermal attributes of the tube bundles are meaningly affected by varying the SCT attack angle. Besides, it is also clear that splitting the CCTs to SCTs leads to increasing the $\overline{Nu_o}$ and f_o, which are continued to increase by increasing the attack angle in the range 0° ≤ α ≤ 60°, then decrease in the range 60° ≤ α ≤ 90°. The average variations of these parameters at different attack angles compared to CCT bundles are demonstrated in Table 3. The reported data assures that the maximum increases in these parameters are 105.1% and 25.6%, respectively, which are attained at the angle of 60°.

Besides the increase in the heat transfer surface area by splitting the tubes, the wake region behind the tubes is decreased, which leads to another increase in the rate of heat transfer. Increasing the base angle further than zero directs the airflow going from the spacing between the bases of the SCTs to meet and mix with the main airflow between the tube, which powerfully raises both the rate of heat transfer and the air pressure drop. As well, the drop in the coefficients of the heat transfer and friction with growing the attack angle of SCTs between 60° and 90° can be accredited to the weakness of the impingements of the airflow leaving the spacing between the bases of the SCTs and the main airflow, which reduces the flow mixing. These conditions may be the reasons for the slowing down the increases in the $\overline{Nu_o}$ and f_o with increasing the angle in this range.

6.2 Thermal performance indicator

To be an effective heat exchange tool, the increase in the heat transfer caused by employing the SCTs should be higher than the associated increase in the fluid pumping power. Many expressions were established by other researchers to evaluate the performance characteristics. In the current analysis, the *TPI* is assessed using St_o and f_o ratios [30] estimated with engaging SCTs and CCTs as the heat transfer surfaces, as follows;

$$TPI = \frac{St_{o,SCT}/St_{o,CCT}}{\left(f_{o,SCT}/f_{o,CCT}\right)^{1/3}} \qquad (15)$$

It is clear that the *TPI* is augmented by growing the attack angle of the SCTs in the range $0° \leq \alpha \leq 60°$, while it is then reduced in the range $60° \leq \alpha \leq 90°$. Besides, there is a slight increase in the *TPI* by increasing the airflow rate. Furthermore, the maximum value of *TPI* is 1.93, recorded at maximum airflow rate and $\alpha = 60°$.

Table 3: Percentage variations in the $\overline{Nu}_o$ and f_o compared to that of CCTs.

Parameter	$\alpha = 0°$	$\alpha = 15°$	$\alpha = 30°$	$\alpha = 45°$	$\alpha = 60°$	$\alpha = 75°$	$\alpha = 90°$
$\overline{Nu}_o$	54.5%	79.3%	85.2%	94.8%	105.1%	57.7%	32.5%
f_o	7.8%	17.2%	19.5%	23.2%	25.6%	18.5%	9.1%
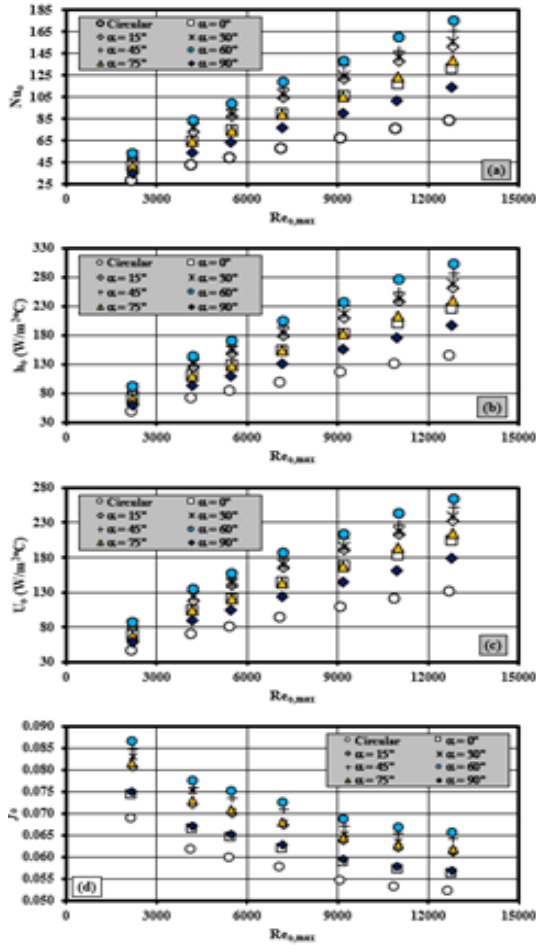
Fig. 7 Results of the experiments ($S_T/d_{t,o}=S_L/d_{t,o}= 2$, $\delta = 0.252$); (a) $\overline{Nu}_o$, (b) $\overline{h}_o$, (c) U_o, (d) f_o.
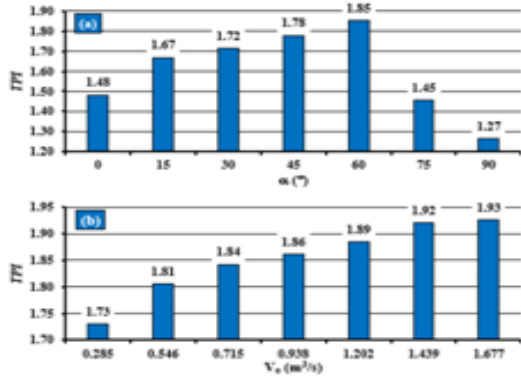

Fig. 8: The resulted *TPI* versus (a) angles, (b) flowrates at $\alpha = 60°$.

7. Summary

This work presents a phase in augmenting the cooling rate of an air cooler by engaging SCTs instead of regular ones. Experiments are carried out for an inline arrangement with contestant spacing in all directions. The main parameters here are the direction of their bases besides the outer flow velocity. The summary of findings is:

- Splitting the tubes augments the heat exchange rate besides increasing the airflow resistance.
- The orientation of the airflow on SCT base varies the cooling rate and pressure decay of the air with two different trends.
  - From angle zero to 60°, the air-cooling rate and pressure decay are increased with widening the angle. Compared with regular tubes, their highest increases are 105.1% and 25.6%, respectively, occurred at $\alpha = 60°$.
  - In the extent, $60° \leq \alpha \leq 90°$, the air-cooling rate and pressure decay are damped with widening the angle. Compared with regular ones, their increases are dropped to be 32.5% and 9.1%, respectively, at $\alpha = 90°$.
- The *TPI* is improved by increasing the angle in the extent $0° \leq \alpha \leq 60°$, to reach 1.93 at $\alpha = 60°$; after this angle, it is reduced.

8 Appendix A

In the existing research, the approach of Kline and McClintock [39] is incorporated to assess the uncertainty in all parameters as follows (maximum values);

$$\frac{\omega_{S_T/d_{t,o}}}{S_T/d_{t,o}} = \pm\sqrt{\left(\frac{\omega_{S_T}}{S_T}\right)^2 + \left(\frac{-\omega_{d_{t,o}}}{d_{t,o}}\right)^2} = \pm\sqrt{\left(\frac{0.01}{23.81}\right)^2 + \left(\frac{-0.01}{15.88}\right)^2} = \pm 0.08\% \quad \text{(A.1)}$$

$$\omega_{S_T-d_{t,o}} = \pm\sqrt{(\omega_{S_T})^2 + (-\omega_{d_{t,o}})^2} = \pm\sqrt{(0.01)^2 + (-0..01)^2} = \pm 0.014 \text{ mm} \quad \text{(A.2)}$$

$$\frac{\omega_{A_{t,o}}}{A_{t,o}} = \pm\sqrt{\left(\frac{\omega_{d_{t,o}}}{d_{t,o}}\right)^2 + \left(\frac{\omega_{L_t}}{L_t}\right)^2} = \pm\sqrt{\left(\frac{0.01}{15.88}\right)^2 + \left(\frac{0.5}{950}\right)^2} = \pm 0.08\% \quad \text{(A.3)}$$

$$\frac{\omega_{A_{t,i}}}{A_{t,i}} = \pm\sqrt{\left(\frac{\omega_{d_{t,i}}}{d_{t,i}}\right)^2 + \left(\frac{\omega_{L_t}}{L_t}\right)^2} = \pm\sqrt{\left(\frac{0.01}{14.45}\right)^2 + \left(\frac{0.5}{950}\right)^2} = \pm 0.09\% \quad \text{(A.4)}$$

$$\frac{\omega_{A_{duct}}}{A_{duct}} = \pm\sqrt{\left(\frac{\omega_W}{W}\right)^2 + \left(\frac{\omega_H}{H}\right)^2} = \pm\sqrt{\left(\frac{0.5}{250}\right)^2 + \left(\frac{0.5}{950}\right)^2} = \pm 0.21\% \quad \text{(A.5)}$$

$$\frac{\omega_{A_{orifice}}}{A_{orifice}} = \pm\sqrt{\left(\frac{2\omega_{d_{orifice}}}{d_{orifice}}\right)^2} = \pm\left(\frac{2*0.5}{101.6}\right) = \pm 0.98\% \quad \text{(A.6)}$$

$$\omega_{\Delta T_w} = \pm\sqrt{(\omega_{T_{w,o}})^2 + (-\omega_{T_{w,i}})^2} = \pm 0.5 * \sqrt{2} = \pm 0.71°C \quad \text{(A.7)}$$

$$\omega_{\Delta T_a} = \pm \sqrt{\left(\omega_{T_{a,i}}\right)^2 + \left(-\omega_{T_{a,o}}\right)^2} = \pm 0.04 * \sqrt{2} = \pm 0.06°C \tag{A.8}$$

$$\omega_{\Delta T_i} = \omega_{\Delta T_o} = \pm \sqrt{\left(\omega_{T_{a,ave,i}}\right)^2 + \left(-\omega_{T_{w,o}}\right)^2} = \pm\sqrt{(0.04)^2 + (0.5)^2} \cong \pm 0.5°C \tag{A.9}$$

$$\omega_{\Delta T_{LM}} = \pm \frac{\omega_T \sqrt{2}}{\ln\left[\frac{\Delta T_i}{\Delta T_o}\right]} \sqrt{2 - 2\Delta T_{LM}\left(\frac{1}{\Delta T_i} + \frac{1}{\Delta T_o}\right) + \Delta T_{LM}^2\left(\frac{1}{\Delta T_i^2} + \frac{1}{\Delta T_o^2}\right)} \tag{A.10}$$

$$\frac{\omega_{u_o}}{u_o} = \pm \sqrt{\left(\frac{0.7566\ \omega_{\Delta H_{orifice}}}{\Delta H_{orifice}}\right)^2 + \left(\frac{\omega_{A_{duct}}}{A_{duct}}\right)^2 + \left(\frac{\omega_{A_{orifice}}}{A_{orifice}}\right)^2} \cong \pm 4.29\% \tag{A.11}$$

$$\frac{\omega_{u_{o,max}}}{u_{o,max}} = \pm \sqrt{\left(\frac{\omega_{u_o}}{u_o}\right)^2 + \left(\frac{\omega_{S_T}}{S_T}\right)^2 + \left(\frac{\omega_{S_T-d_{t,o}}}{S_T - d_{t,o}}\right)^2} \cong \pm 4.29\% \tag{A.12}$$

$$\frac{\omega_{Re_{o,max}}}{Re_{o,max}} = \pm \sqrt{\left(\frac{\omega_{u_{o,max}}}{u_{o,max}}\right)^2 + \left(\frac{\omega_{d_{t,o}}}{d_{t,o}}\right)^2 + \left(\frac{\omega_{v_o}}{v_o}\right)^2} \cong \pm 4.29\% \tag{A.13}$$

$$\frac{\omega_{\dot{V}_o}}{\dot{V}_o} = \pm \frac{0.7566\ \omega_{\Delta H_{orifice}}}{\omega_{\Delta H_{orifice}}} = \pm 0.32\% \tag{A.14}$$

$$\frac{\omega_{\dot{m}_o}}{\dot{m}_o} = \pm \sqrt{\left(\frac{\omega_{\dot{V}_o}}{\dot{V}_o}\right)^2 + \left(\frac{\omega_{\rho_o}}{\rho_o}\right)^2} = \pm 0.33\% \tag{A.15}$$

$$\omega_{\dot{V}_w} = \pm \sqrt{\left(\frac{1}{1} * 0.01\right)^2 + \left(\frac{-50}{1^2} * \left(\frac{1}{60}\right)\right)^2} = \pm 0.8334 \ l/min = \pm 1.67\% \tag{A.16}$$

$$\frac{\omega_{\dot{m}_w}}{\dot{m}_w} = \pm \sqrt{\left(\frac{\omega_{\rho_w}}{\rho_w}\right)^2 + \left(\frac{\omega_{\dot{V}_w}}{\dot{V}_w}\right)^2} = \pm\sqrt{(0.001)^2 + (0.0167)^2} = \pm 1.67\% \tag{A.17}$$

$$\frac{\omega_{Re_i}}{Re_i} = \pm \sqrt{\left(\frac{\omega_{\dot{m}_w}}{\dot{m}_w}\right)^2 + \left(\frac{\omega_{d_{t,h}}}{d_{t,h}}\right)^2 + \left(\frac{\omega_{\mu_i}}{\mu_i}\right)^2} \cong \pm 1.67\% \tag{A.18}$$

$$\frac{\omega_{Q_o}}{Q_o} = \pm \sqrt{\left(\frac{\omega_{\dot{m}_o}}{\dot{m}_o}\right)^2 + \left(\frac{\omega_{Cp_o}}{Cp_o}\right)^2 + \left(\frac{\omega_{\Delta T_a}}{\Delta T_a}\right)^2} \tag{A.19}$$

$$\frac{\omega_{Q_i}}{Q_i} = \pm \sqrt{\left(\frac{\omega_{\dot{m}_i}}{\dot{m}_i}\right)^2 + \left(\frac{\omega_{Cp_i}}{Cp_i}\right)^2 + \left(\frac{\omega_{\Delta T_w}}{\Delta T_w}\right)^2} \tag{A.20}$$

$$\omega_{Q_{ave}} = \pm \frac{1}{2}\sqrt{\left(\omega_{Q_o}\right)^2 + \left(\omega_{Q_i}\right)^2} \tag{A.21}$$

$$\frac{\omega_{U_o}}{U_o} = \pm \sqrt{\left(\frac{\omega_{Q_{ave}}}{Q_{ave}}\right)^2 + \left(\frac{-\omega_{A_{t,o}}}{A_{t,o}}\right)^2 + \left(\frac{-\omega_{\Delta T_{LM}}}{\Delta T_{LM}}\right)^2} \tag{A.22}$$

$$\frac{\omega_{\overline{Nu}_i}}{\overline{Nu}_i} = \pm \sqrt{\left(\frac{0.8\ \omega_{Re_i}}{Re_i}\right)^2 + \left(\frac{0.4\ \omega_{Pr_i}}{Pr_i}\right)^2} \cong \pm 1.34\% \tag{A.23}$$

$$\frac{\omega_{\overline{h}_i}}{\overline{h}_i} = \pm \sqrt{\left(\frac{\omega_{\overline{Nu}_i}}{\overline{Nu}_i}\right)^2 + \left(\frac{\omega_{k_i}}{k_i}\right)^2 + \left(\frac{-\omega_{d_{t,h}}}{d_{t,h}}\right)^2} \cong \pm 1.35\% \tag{A.24}$$

$$\omega_{\overline{h}_o} = \pm \sqrt{\left(\frac{\partial \overline{h}_o}{\partial U_o}\omega_{U_o}\right)^2 + \left(\frac{\partial \overline{h}_o}{\partial A_{t,o}}\omega_{A_{t,o}}\right)^2 + \left(\frac{\partial \overline{h}_o}{\partial A_{t,i}}\omega_{A_{t,i}}\right)^2 + \left(\frac{\partial \overline{h}_o}{\partial \overline{h}_i}\omega_{\overline{h}_i}\right)^2} \tag{A.25}$$

$$\frac{\omega_{\overline{Nu}_o}}{\overline{Nu}_o} = \pm \sqrt{\left(\frac{\omega_{\overline{h}_o}}{\overline{h}_o}\right)^2 + \left(\frac{\omega_{d_{t,o}}}{d_{t,o}}\right)^2 + \left(\frac{-\omega_{k_o}}{k_o}\right)^2} \tag{A.26}$$

$$\frac{\omega_{f_o}}{f_o} = \pm \sqrt{\left(\frac{\omega_{\Delta P_o}}{\Delta P_o}\right)^2 + \left(\frac{\omega_{\rho_o}}{\rho_o}\right)^2 + \left(\frac{-2\omega_{u_{o,max}}}{u_{o,max}}\right)^2} \tag{A.27}$$

$$\frac{\omega_{St_o}}{St_o} = \pm \sqrt{\left(\frac{\omega_{\overline{Nu}_o}}{\overline{Nu}_o}\right)^2 + \left(\frac{\omega_{Re_{o,max}}}{Re_{o,max}}\right)^2 + \left(\frac{-\omega_{Pr_o}}{Pr_o}\right)^2} \tag{A.28}$$

$$\frac{\omega_{TPI}}{TPI} = \pm \sqrt{\left(\frac{\omega_{St_{o,SCT}}}{St_{o,SCT}}\right)^2 + \left(\frac{\omega_{St_{o,CCT}}}{St_{o,CCT}}\right)^2 + \left(\frac{\frac{1}{3}\omega_{f_{o,SCT}}}{f_{o,SCT}}\right)^2 + \left(\frac{\frac{1}{3}\omega_{f_{o,CCT}}}{f_{o,CCT}}\right)^2} \tag{A.29}$$

References

[1] M.R. Salem, "Experimental investigation on the hydrothermal attributes of MWCNT/water nanofluid in the shell-side of shell and semi-circular tubes heat exchanger", Applied Thermal Engineering, vol. 176, Article no. 115438, 2020.

[2] T.L. Bergman, A.S. Lavine, F.P. Incropera and D.P. Dewitt, "Fundamentals of Heat and Mass Transfer", 7th edition, John Wiley & Sons, 2011.

[3] M.R. Salem, K.M. Elshazly, R.Y. Sakr, R.K. Ali, Experimental study on convective heat transfer and pressure drop of water-based nanofluid inside shell and coil heat exchanger, PhD dissertation, Faculty of Engineering at Shoubra, Benha University, 2014.

[4] A.P. Colburn, "A method of correlating forced convection heat transfer data and a comparison with fluid friction", Transactions of the American Institute of Chemical Engineers, vol. 29, pp. 174-210, 1933.

[5] O.L. Pierson, "Experimental investigation of the influence of tube arrangement on convection heat transfer and flow resistance in cross flow of gases over tube banks", Transactions of ASME, vol. 59, pp. 563-572, 1937.

[6] G.A. Omohundro, O.P. Bergelin, A.P. Colburn, "Heat transfer and fluid friction during flow across banks of tubes", ASME Journal of Heat Transfer, vol. 71, pp. 27-34, 1949.

[7] O.P. Bergelin, G.A. Brown, H.L. Hull, F.W. Sullivan, "Heat transfer and fluid friction during flow across banks of tubes - III: A study of tube spacing and tube size", ASME Journal of Heat Transfer, vol. 72, pp. 881-888, 1950.

[8] C.E. Jones, E.S. Monroe, "Convection heat transfer and pressure drop of air flowing across in-line tube banks: Part I - apparatus, procedures, and special effects", ASME Journal of Heat Transfer, vol. 80, pp. 18-24, 1958.

[9] A. Zukauskas, "Heat transfer from tubes in crossflow", Advances in Heat Transfer, vol. 8, pp. 93-160, 1972.

[10] M. Jakob, "Heat transfer and flow resistance in cross flow of gases over tube banks", Trans. ASME, vol. 60, p. 384, 1938.

[11] L.A.M. Endres, S.V. Möller, "On the fluctuating wall pressure field in tube banks", Nuclear Engineering and Design, vol. 203(1), pp. 13-26, 2001.

[12] K. Torii, K.M. Kwak, K. Nishino, "Heat transfer enhancement accompanying pressure-loss reduction with winglet-type vortex generators for fin-tube heat exchangers", International Journal of Heat and Mass Transfer, vol. 45, pp. 3795-3801, 2002.

[13] Y.L. He, W.Q. Tao, F.Q. Song, W. Zhang, "Three-dimensional numerical study of heat transfer characteristics of plain plate fin-and-tube heat exchangers from view point of field synergy principle", International Journal of Heat and Fluid Flow, vol. 26, pp. 459-473, 2005.

[14] M. Moawed, "Thermal performance of a cross flow heat exchanger with semi-circular tubes", ERJ Shoubra Faculty of Engineering, vol. 4, pp. 87-109, June 2005.

[15] E.Z. Ibrahiem, A.O. Elsayed, "Heat transfer performance of a semi-circular tube bank", Heat Transfer Research, vol. 46(6), pp. 563-576, 2015.

[16] S. Liu, L. Wang, J. Fan, Y. Zhang, Y. Dong, K. Song, "Tube transverse pitch effect on heat/mass transfer characteristics of flat tube bank fin mounted with vortex generators", Journal of Heat Transfer, vol. 130(6), article no. 064502 (3 pages), 2008.

[17] M. Odabaee, K. Hooman, "Metal foam heat exchangers for heat transfer augmentation from a tube bank", Applied Thermal Engineering, vol. 36, pp. 456-463, 2012.

[18] A.M. Lavasani, H. Bayat, T. Maarefdoost, "Experimental study of convective heat transfer from in-line cam shaped tube bank in crossflow", Applied Thermal Engineering, vol. 65, pp. 85-93, 2014.

[19] Z. Lin, L. Wang, Y. Zhang, "Numerical study on heat transfer enhancement of circular tube bank fin heat exchanger with interrupted annular groove fin", Applied Thermal Engineering, vol. 73, 1465-1476, 2014.

[20] A. Lavasani, H. Bayat, T. Maarefdoost, "Experimental study of convective heat transfer from in-line cam shaped tube bank in crossflow", Applied Thermal Engineering, vol. 65, pp. 85-93, 2014.

[21] C. Wang, K. Chen, J. Liaw, C. Tseng, "An experimental study of the air-side performance of fin-and-tube heat exchangers having plain, louver, and semi-dimple vortex generator configuration", International Journal of Heat and Mass Transfer, vol. 80, pp. 281-287, 2015.

[22] E. Tian, Y. He, W. Tao, "Numerical simulation of finned tube bank across a staggered circular-pin-finned tube bundle", Numerical Heat Transfer, Part A, vol. 68, pp. 737–760, 2015.

[23] K. Song, Z. Xi, M. Su, L. Wang, X. Wu, L. Wang, "Effect of geometric size of curved delta winglet vortex generators and tube pitch on heat transfer characteristics of fin-tube heat exchanger", Experimental Thermal and Fluid Science, vol. 82, pp. 8-18, 2017.

[24] M. Ahmed, M. Yaseen, M. Yusoff, "Numerical study of convective heat transfer from tube bank in cross flow using nanofluid", Case Studies in Thermal Engineering, vol. 10, pp. 560-569, 2017.

[25] J. Xu, J. Li, Y. Ding, Q. Fu, M. Cheng, Q. Liao, "Numerical simulation of the flow and heat-transfer characteristics of an aligned external three-dimensional rectangular-finned tube bank", Applied Thermal Engineering, vol. 145, pp. 110–122, 2018.

[26] W. Dang, J. Nugud, Z. Lin, Y. Zhang, S. Liu, L. Wang, "The performances of circular tube bank fin heat exchangers with fins punched with quadrilateral vortex generators and flow re-distributors", Applied Thermal Engineering, vol. 134, pp. 437-449, 2018.

[27] B. Lotfi, B. Sundén, "Development of new finned tube heat exchanger: Innovative tube-bank design and thermohydraulic performance", Heat Transfer Engineering, vol. 41(14), p.p.1209-1231, 2020.

[28] K. Lindqvist, E. Naess, "On correction factors in thermal-hydraulic correlations for compact fin-tube bundles", Heat Mass Transfer, vol. 56, pp. 1713-1723, 2020.

[29] M.R. Salem, M.B. Eltoukhey, R.K. Ali, K.M. Elshazly, "Experimental investigation on the hydrothermal performance of a double-pipe heat exchanger using helical tape insert", International Journal of Thermal Sciences, vol. 124, pp. 496-507, 2018.

[30] K.M. Elshazly, R.Y. Sakr, R.K. Ali, M.R. Salem, "Effect of γ-Al$_2$O$_3$/water nanofluid on the thermal performance of shell and coil heat exchanger with different coil torsions", Heat and Mass Transfer, vol. 53 (6), 1893-1903, 2017.

[31] M.R. Salem, "Performance enhancement of a vapor compression refrigeration system using R134a/MWCNT-oil mixture and liquid-suction heat exchanger equipped with twisted tape turbulator", International Journal of Refrigeration, vol. 120, 357-369, 2020.

[32] S.M. Elshamy, M.T. Abdelghany, M.R. Salem, O.E. Abdellatif, "Based Al$_2$O$_3$ nanofluid including diverse coil geometries: An experimental study", Journal of Nanofluids, vol. 9 (1), 13-23, 2020.

[33] M.R. Salem, H.A. El-Gammal, A.A. Abd-Elaziz, K.M. Elshazly, "Study of the performance of a vapor compression refrigeration system using conically coiled tube-in-tube evaporator and condenser", International Journal of Refrigeration, vol. 99, 393-407, 2019

[34] H.A. Refaey, E. Specht, M.R. Salem, "Influence of fuel distribution and heat transfer on energy consumption in tunnel kilns", International Journal of Advances in Engineering & Technology (IJAET), vol. 8(3), 281-293, 2015.

[35] R.W. Miller, "Flow measurement engineering handbook", 3rd edition, New York: McGraw-Hill, 2000.

[36] R.K. Shah, D.P. Sekulić, "Fundamentals of heat exchanger design", 6th edition, Hoboken, NJ: John Wiley & Sons, p. 189, 2003.

[37] V. Gnielinski, "New equations for heat and mass transfer in turbulent pipe and channel flow", International Chemical Engineering, vol. 16, pp. 359-368, 1976.

[38] G.K. Filonenko, "Hydraulic resistance of pipes (Hydraulischer Widerstand von Rohrleitungen)," Teploenergetika, vol. 1(4), pp. 40-44, 1954.

[39] S.J. Kline, F.A. McClintock, "Describing uncertainties in single-sample experiments", Mechanical Engineering, vol. 75(1), pp. 3-8, 1953.

Nomenclatures		**Greek letters**	
A	Area, m^2	α	Attack angle, °
Cp	Specific heat, $J/kg.°C$	ρ	Density, kg/m^3
d	Diameter, m	**Superscripts and subscripts**	
f	Fanning friction factor	ave	Average
h	Convection heat transfer coefficient, $W/m^2.°C$	b	Base
k	Thermal conductivity, $W/m.°C$	c	Cross-sectional
L	Length, m	cir	Circular
$\dot{m}$	Mass flow rate, kg/s	h	Hydraulic
P	Pressure, Pa	i	Inner or inlet or internal
Q	Heat transfer rate, W	LM	Logarithmic Mean
S	Spacing between the bases of two adjacent SCTs, m	m	Mean
		max	Maximum
T	Temperature, °C or K	o	Out or outer
u	Velocity, m/s	s	Surface
$\dot{V}$	Volume flow rate, m^3/s	t	Tube
Dimensionless groups		**Acronyms and abbreviations**	
$\overline{Nu}$	Average Nusselt number	CCT	Complete Circular Tube
Pr	Prandtl number	SCT	Semi-Circular Tube
Re	Reynolds number	TPI	Thermal Performance Indicator
St	Stanton number		